Development of Slurry-Jet Erosion Test for Elastomeric Materials

Wichain Chailad[1], Liu Yang*[1], Vince Coveney[2], Chris Bowen[2], Alan Bickley[1]

[1] Department of Mechanical and Aerospace Engineering, University of Strathclyde, Glasgow, UK

[2] Department of Mechanical Engineering, University of Bath, Bath, UK

*Corresponding author E-mail address: l.yang@strath.ac.uk

Abstract

This article presents the development of a slurry-jet erosion test rig and characterisation procedure for slurry erosive wear behaviour of elastomeric materials. Key parameters such as the mass of impacting particles, particle concentrations, impact angles, and slurry velocities can be set and controlled accurately by following an established measurement protocol. The results for slurry velocity, concentration, and temperature showed an excellent control using the test rig. The test rig was designed to maintain the slurry temperature change within ±2°C as required by BS/ISO 23529 and no additional cooling system is needed. Characteristics of silica sand particles in the slurry experienced very little change after several test batches in terms of average particle size, particle distribution, and angularity. Commissioning of the rig was carried out by evaluating erosion behaviour of polychloroprene rubber with the variation of mass of erodent particles and impact angles. The results showed that the developed erosion test rig and testing procedure were reliable for investigating slurry erosive wear processes of elastomers. Erosive wear resistance of different elastomers to slurry-jet erosion can be investigated under varied test parameters. The experimental erosion wear results were compared with calculated values using the theoretical models of cutting and deformation wear.

Keywords: Slurry erosion, Polymers, Mining, Erosion testing

This is a peer-reviewed, accepted author manuscript of the following article: Chailad, W., Yang, L., Coveney, V., Bowen, C., & Bickley, A. (2021). Development of slurry-jet erosion test for elastomeric materials. Wear, [204125]. https://doi.org/10.1016/j.wear.2021.204125

1. Introduction

Over the past decades, slurry transport systems have been widely used to transport ores, sand, and tailings in mining operations. They offer economical, environmental and handling advantages over railroad transport, especially when mines are located in extremely remote areas. During the slurry transport process, erodent particles such as ore or tailing, suspended in the water or oil, are pumped over a distance through a pipeline. This leads to extensive mechanical interactions between these particles and slurry processing equipment, including pumps, pipe bends, and elbows. As a result, these components tend to suffer from severe erosive wear with a reduced lifetime. In order to address this challenge, wear-resistant materials are typically employed as a sacrificial liner to protect the equipment from rapid erosion damage. It has been shown that elastomers tend to have an excellent erosion resistance [1–6] compared to the other types of materials due to their abilities to deform to a large extent without damage and high rebound resilience to deflect the impact energy from the impinging particles. Consequently, highly resilient rubber lining materials have been widely used to extend the lifetime of pipes, pumps, hoses and valves against erosion by hard particles in mining industries.

Despite good wear resistance of rubber liners, improving their slurry erosion resistance can help to reduce equipment downtime for replacing with new liners and in turn, save operation and maintenance costs. An improved understanding of the erosion process of rubber lining would improve the use of lining materials more effectively and encourage further development of the elastomeric materials for erosion protections. Some progress has been made towards fully characterising and understanding rubber erosion in dry conditions, such as air-borne particles [1,7–10]. However, there has been little progress reported thus far for rubber erosion under wet slurry conditions relevant to slurry transportation in mining industry.

To our best knowledge, there are no standard test methods for characterising slurry erosion of elastomer materials. Nevertheless, several researchers have attempted to design and build their own test rigs in order to investigate the slurry erosion under different operating conditions. As a result, different test rigs has been

developed including slurry pot test rig [11–13], Coriolis erosion test rig [14–16], whirling arm test rig [17] and jet-type test rig [13,18,19]. The slurry pot test rig has limited control and tracking of main parameters such as the dispersion, concentration and degradation of erodent particles, the impact velocity and slurry temperature. Coriolis test rig can provide results quickly; however the impact angle cannot be varied in a wide range. Whirling arm test rig is developed mostly to simulate specific slurry erosion conditions rather than for modelling erosion mechanisms. The slurry-jet erosion test (SJET) rig is considered in this work as it offers an alternative to the techniques described above. The jet-type apparatus is simple in design, low in construction cost, and easy to operate. The test specimen can be varied in dimension regarding the test conditions and materials. The key parameters affecting the erosive wear of materials can be controlled and determined.

The SJET rigs can be mainly categorised into two main groups, namely recirculation and non-recirculation. Table 1 summarises the key aspects of SJET rigs and their applicability found in the literature

Table 1 Summary of slurry-jet erosion tests found in the literature

Type	Target material	Particle size (μm)	Sample size			Maximum velocity (m/s)	Particle content (wt.%)	Nozzle diameter (mm)	Reference
			Width (mm)	Length (mm|)	Thickness (mm)				
Semi recirculation	Aluminium and copper	425-1000	30	35	3-5	8	30	4.5-6.5	[13]
Recirculation	Ni(200)	88-150	Φ 0.75		10	30	30	2	[20]
Recirculation	Aluminium and glass	200-300	26	25	10	17	20	4.76	[19]
Semi recirculation	Aluminium	600-850	35	30	3-5	4.5	19	5.5	[21]
Semi recirculation	Aluminium	600-850	15	10	N/A	3.6	15	5.5	[22]
Recirculation	W-Co-Cr-C coated on stainless steel	135-235	50	50	10	26	2.1	6.15-25.5	[23]
Recirculation	Elastomers, polymers, cast iron	42-415	30	20	5	25	0.1-7	3	[18]
Semi recirculation	Ceramic materials, alumina	600-850	25	20-25	3-5	7.3	3-7.5	3.7	[24]
Semi recirculation	304L stainless	400-650	20	20	N/A	3.4	13.2	4.5	[25]
Recirculation	Steel	420	40-68	22-40	5-6	27	1.36	Variable	[26]
Non-recirculation	Aluminium and cast iron	25-500	20	20	5	25	1	4	[27]
Non-recirculation	Coated on hydro turbine steel, CA6NM	>300		N/A		4	0.1 and 0.5	N/A	[28]
Non-recirculation	Coated Hydro turbine steel, CA6NM	>300		N/A		16	0.1	N/A	[29]
Recirculation	Steels, elastomers, plastics, cast irons, ceramics, cermets, overlays	212-300		N/A		16	10	5	[3]
Recirculation	Elastomers, plastics and steels	250-500		N/A		25	20	N/A	[6]

The slurry is circulated continuously in a recirculation system whereas the erodent particles are separated from a non-recirculation system after impacting the target material so that the carrier liquid flows through the pump without erodent particles. The latter can minimise the pump wear and erodent particle degradation. However, the non-recirculating rig is more complicated to construct and operate as the ejector needs to calibrate prior testing, and rig performance is susceptible to its structure and geometry. There is a complex interaction between slurry velocity and concentration of erodent particles. Therefore, several studies used the recirculating rigs [18–20,23,26]. However, continuous circulation of the flowing media causes a temperature rise accelerating water evaporation and in turn changing slurry composition. This is particularly problematic to a small slurry reservoir and impose a significant concern for testing elastomeric materials, whose properties are sensitive to a temperature change. An active temperature control can mitigate this issue but this leads to an additional cost.

Several SJET rigs have been applied to investigate the erosive wear of materials and coatings, as seen in Table 1; interestingly, none of them was developed primarily for elastomers. In these rigs, the flowing liquid was circulated continuously, and its temperature was not controlled strictly, making it be not suitable to use for elastomeric materials. Although elastomers have been investigated by some work with slurry-jet erosion tests, details of rig construction were lacking, and changes of slurry temperature during testing were not monitored. Thus, this study provides the new development of the SJET rig with the ability to accurately simulate and control the test conditions for slurry erosive wear of elastomers efficiently.

2. Design of slurry-jet erosion test rig

The SJET rig developed in this work was designed to investigate the effect of a wide range of parameters relevant to slurry erosion of elastomeric materials. The key parameters for testing include slurry velocity and impact angle, particle size, shape, and concentration, standoff distance between the nozzle outlet and target surface, and slurry temperature. The test system should have the ability to control and monitor these conditions accurately while it ensures a lab investigation of the elastomer wear in a harsh mineral processing

environment. As a consequence, the following requirements should be met. The SJET rig needs to have the ability to conduct an erosion test in a large amount of slurry at each test batch. The slurry temperature must be well defined and controlled. The sand particles need to be dispersed uniformly during testing to ensure the consistency of slurry composition throughout the test period. Moreover, the SJET rig needs to facilitate a wide range of slurry velocities and impact angles with high accuracy.

For our SJET rig, a large double tank layout can facilitate the slurry erosion tests with a large volume of the slurry without recirculation. The increase in the slurry temperature can be minimised simultaneously due to large batch operation. In addition, the problem of controlling and monitoring the concentration of the erodent particles in the slurry due to fluid evaporation and particle change as found in a recirculation system can also be eliminated in our rig design. Instead of introducing the erodent particles into the complicated nozzle design and mixing with the fluid before impacting the specimen, the erodent particles are mixed with the liquid and dispersed sufficiently by a high-performance agitator in our design. The well-dispersed slurry can be then pumped to impinge rubber specimens. A high-speed pump and an inverter enable varying slurry velocities with accurate control. Different impact angles can be kept constant throughout each testing phase using interchangeable specimen holders. The standoff distance is also adaptable and can be maintained through a robust nozzle and a specimen holder.

Figure 1 presents a schematic diagram of the SJET rig developed in the present work.

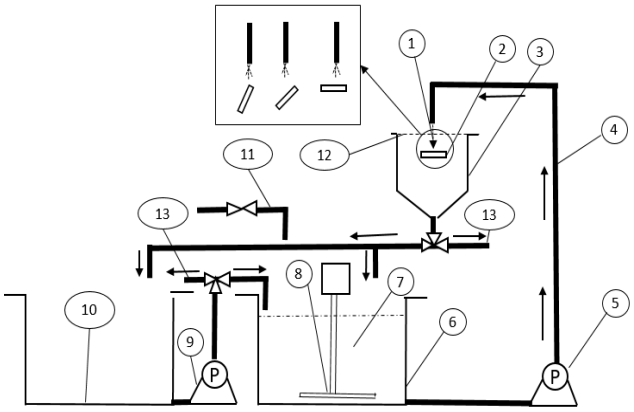

1. Nozzle (internal diameter 4mm)
2. A test piece with backing strip (adjustable angle 10 to 90 degrees)
3. Slurry collecting reservoir
4. Main slurry pipes
5. Main pump with inverter
6. Working slurry reservoir
7. Test liquid (Erodent particles in water)
8. Stirrer/Mixer
9. Transfer pump
10. Slurry storage reservoir
11. Water inlet
12. Splash cover
13. Draining pipe points

Figure 1 Schematic view of the developed slurry-jet erosion test rig (not to scale)

Two large reservoirs of 500 L are used to contain test slurry (6) and to collect slurry (10) after impingement respectively. Using two large parallel-sided reservoirs can facilitate the batch operation, maintain slurry temperature without any active temperature control, and monitor erodent particle concentration and size degradation. Moreover, the slurry temperature can be purposefully adjusted in the slurry storage reservoir (10) if necessary. The testing vessel (3) is used to catch slurry after impingement, and its cover (12) prevents any slurry splash. The stirrer (8) with high motor speed located on the top of the slurry tank (6) ensures uniformity of the erodent particles in the slurry throughout the erosion test duration. The slurry transfer pump (5) can give the slurry velocity at the nozzle output up to 30 m/s. Slurry-jet velocity can be controlled and varied by an external inverter. A specimen can be orientated between 10° and 90° with respect to the direction of the slurry jet by changing the angle of the specimen holder (2). The impact distance between the nozzle and the surface of the specimen can also be adjusted. Thus, the effect of impact distance, including the particle flux rate, can be studied by this rig. The sample can be firmly clamped to the sample holder to eliminate vibration and associated energy dissipation during the test. During testing, the slurry

strikes the sample held in the air in order to eliminate any interference from sample surroundings. The impacting sands are collected by the volumetric column located in the storage reservoir (10), enabling the measurement of their volume and transfer to the testing tank (6) for the next test batch.

3. Evaluation of slurry-jet erosion test rig

3.1 Slurry velocity

The slurry velocity as a function of pump frequency was established by repeating the process three times for each frequency. The method used to determine the slurry velocity involved collecting the slurry from the nozzle outlet into a volumetric beaker. The collected slurry volume was then divided by the time of sampling and cross-sectional area of the nozzle exit to obtain slurry velocity using Equation (1).

$$\text{Slurry velocity (m/s)} = \frac{V_{SL}}{t_S \cdot A_N} \qquad (1)$$

where V_{SL} is collected slurry volume (m^3), t_S is the sampling time (s), and A_N is a nozzle area (m^2). Alternatively, one could also determine the average impact velocity over the whole batch operation using Equation (2).

$$\text{Average slurry velocity (m/s)} = \frac{\overline{V_S}}{t_B \cdot A_N} \qquad (2)$$

where $\overline{V_S}$ is the collected slurry volume in a storage tank (m^3) and t_B is the batch operating time (s).

Figure 2 shows the slurry velocities calculated by Equation (1) as a function of pump frequency. The results are also compared to the slurry velocities calculated by Equation (3) obtained by pump calibration.

$$\text{Slurry velocity (m/s)} = 0.693f\text{-}0.828 \qquad (3)$$

where f is the frequency of the pump.

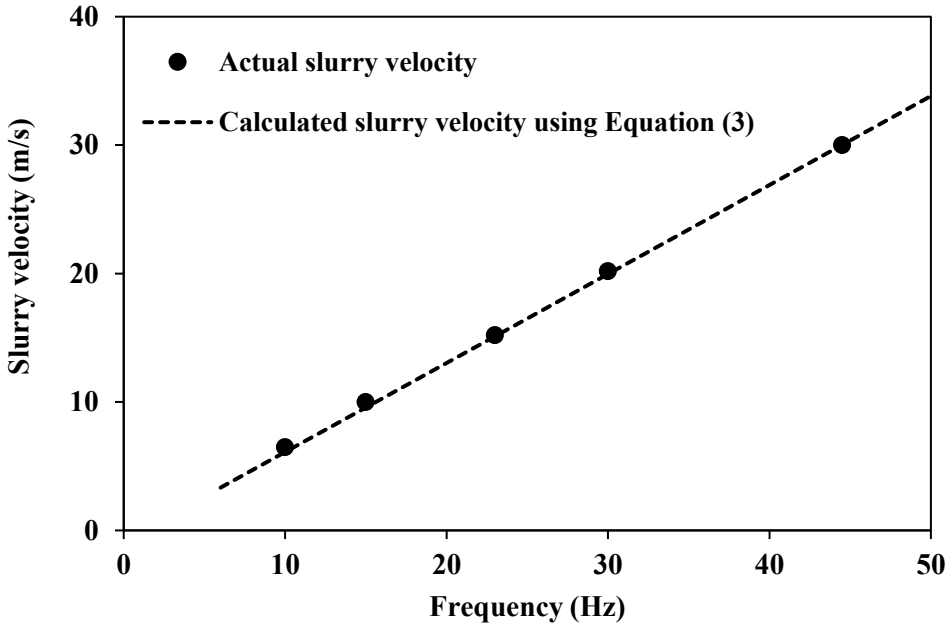

Figure 2 Slurry velocity as a function of inverter frequency for the SJET rig

Figure 2 shows that the measured slurry velocity is linearly proportional to the pump frequency. This has an excellent agreement with the velocity-frequency relationship predicted by Equation (3). As a result, it is a viable approach to use velocity-frequency calibration obtained from a pump to accurately control slurry velocity in our rig. This approach should be used with precaution when applied to a different rig setup as Equation (3) is an empirical correlation specifically for the rig developed in this work and will be likely to be different for different rig configurations. Nevertheless, the results in Figure 2 encourage a beneficial practice that should be commonly considered for establishing a robust control of slurry velocity.

Another aspect of speed control concerns its variation or fluctuation during repeated test batches. This is crucial to understand as most erosion testing require cyclic operation, which might alter the rig pristine conditions and lead to erroneous results. Figure 3 presents the measured slurry velocities during 355 repeated test batches, during which the pump was set to produce a slurry flow of 30 m/s in the rig.

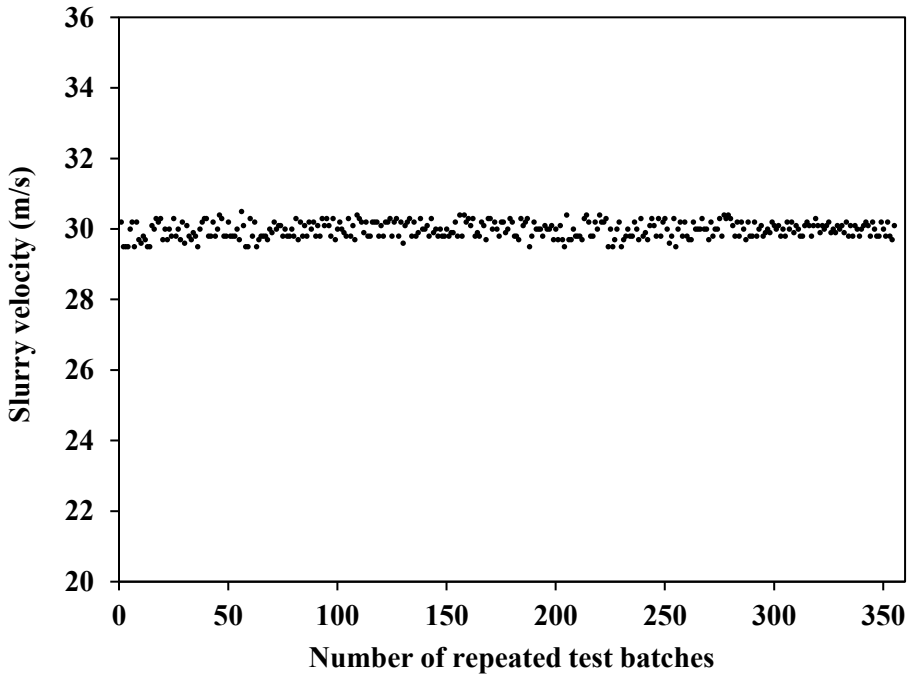

Figure 3 Slurry velocity measured during 355 repeated tests at a set velocity of 30 m/s

As can be seen, the slurry velocities maintained a narrow range around the set speed and the average slurry velocity was found to be 29.98±0.23 m/s. A student's t-test at 95% confidence level was carried out to determine if there was a statistically significant difference between slurry velocities from the set and actual values. The statistical significance (p-value) was found to be 0.07and the discrepancy between the set and actual slurry velocities were not statistically significant throughout the test batches.

3.2 Sand content

In order to measure sand content in the slurry, sand particles collected from the volumetric beaker dried out and subsequently weighed. The measured sand weight, M_S, was further divided by the total weight of slurry, M_{SL}, to gain the weight fraction of sand as in Equation 4.

$$\text{Sand content (wt\%)} = \frac{M_S}{M_{SL}} \cdot 100 \qquad (4)$$

As with slurry velocity, one could also determine average sand content over onewhole batch operation using Equation 5.

$$\text{Average sand concentration (wt\%)} = \frac{\overline{M_{ST}}}{\overline{M_{SL}}} \cdot 100 \qquad (5)$$

where $\overline{M_{ST}}$ is the mass of collected sand in the storage tank, $\overline{M_{SLT}}$ is the mass of collected slurry in the storage tank.

The influence of the slurry velocity on the sand concentration of slurry jet was studied. The sand content in the slurry reservoir was kept at 5wt% and slurry velocities were varied by changing the pump frequency according to Equation (3). For each velocity, three individual batches were tested and the sand concentration was obtained by Equation (5). The results in Figure 4 show that the sand concentration in the slurry as a function of different slurry velocities and the error bar represents 95% confidence limit of the measurement. It can be seen that there seems to be a slight downward trend in the sand content as the slurry velocity increases. However, the linear coefficient is very small and the sand content varies by 0.12% on average from 10 m/s to 30 m/s. In addition, extrapolation of this trend gives 5.1wt% at zero slurry velocity and this agrees well with the sand content in the storage tank. . Thus, it is reasonable to conclude that the dependence of sand concentration on the slurry velocity is negligible for the investigated slurry velocities using our SJET rig.

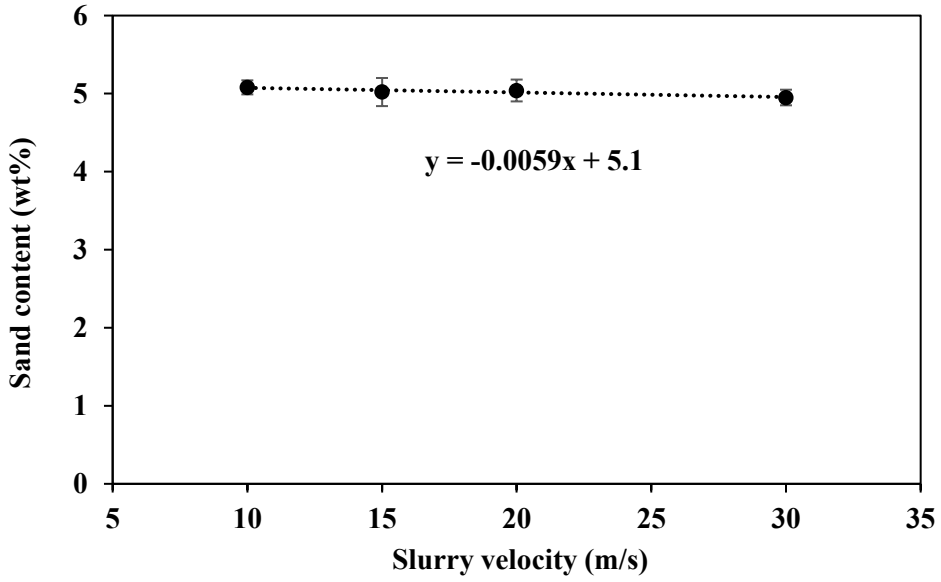

Figure 4 Sand content measured at different slurry velocities under a set sand content of 5wt%

Error! Reference source not found. shows the average sand content calculated using Equation 5.

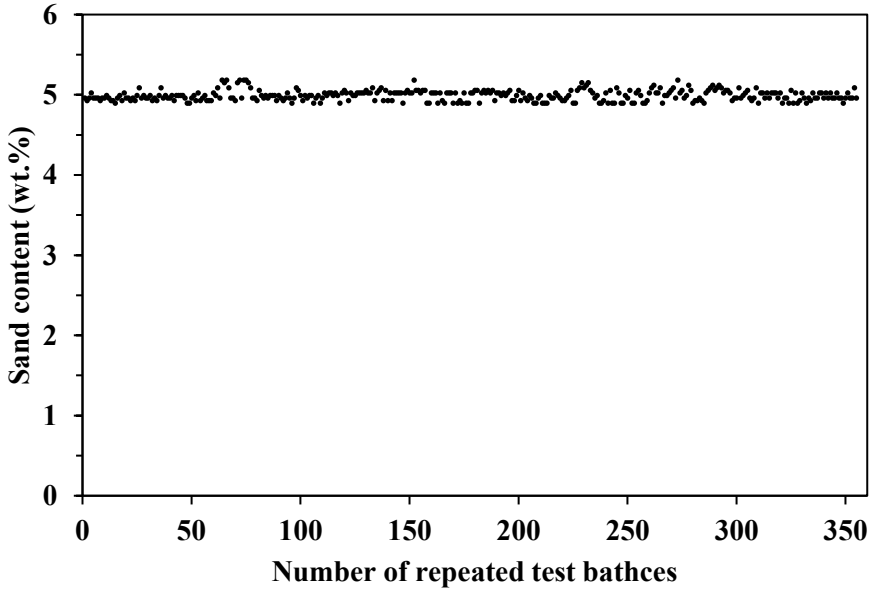

Figure 5 Average sand content during 355 repeated test batches under a set sand content of 5wt%.

It can be seen that the measured sand content agrees well with the set target of 5wt% and the maximum and minimum values obtained from 355 repeated tests are 5.2 and 4.9wt% respectively. Statistical analysis further showed an average value of 4.98 ± 0.07 wt% witha p-value of 0.05.

3.3 Slurry temperature

The slurry temperature was measured during each batch testing containing 400 L of slurry with a slurry velocity of 30 m/s and a sand concentration of 5 wt%. The temperature of the slurry contained in the storage tank was measured using a digital laser IR thermometer immediately after each batch test before the next batch-test commence. Three repeated measurements were conducted at each slurry volume processed by the rig and the results are shown in Figure 6 along with the error bar of 95% confidence limit (too small to be seen).

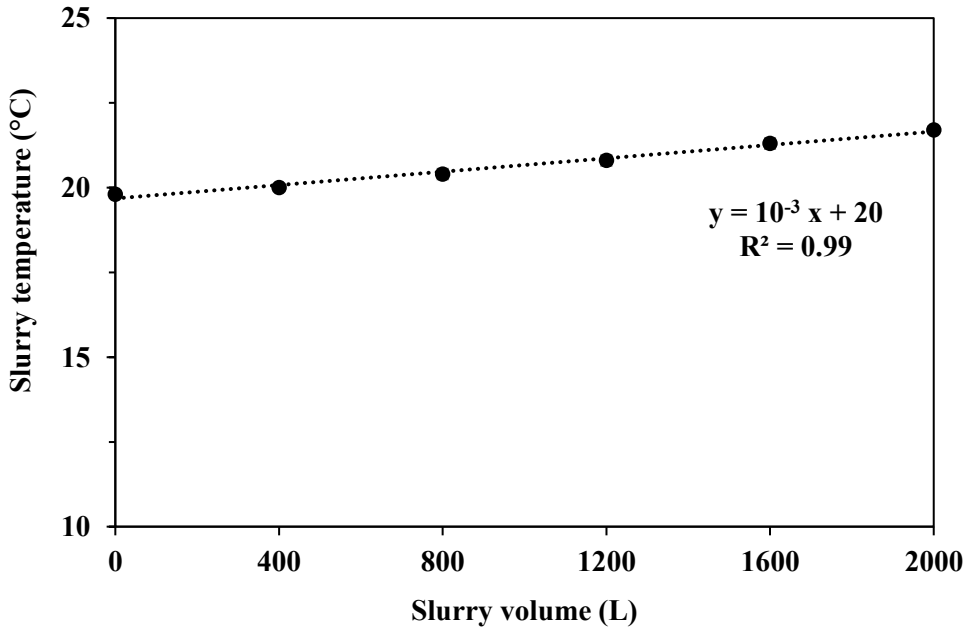

Figure 6 Slurry temperature change as a function of slurry volume processed during erosion test

As can be seen, there is a linear correlation between slurry volume processed during testing and slurry temperature. The slurry temperature increased at a rate 0.001°C/L of processed slurry and reached 2°C

change after processing 2000 L. This is in line with the guidance required by BS/ISO 23529 if the slurry is used less than 2300 L continuously at the maximum velocity.

3.4 Sand size distribution and angularity

During slurry-jet erosion testing, size and shape of sand particles may change after repeatedly passing through the pump and impinging on the specimen. In order to examine this possibility, 40 batch tests were carried out using a slurry of 5wt% at a velocity of 30 m/s and sand particles were randomly sampled after the 1st, 10th, 20th, 30th, and 40th test. The sampled sand particles were then measured to obtain their size distribution.

Figure 7 (a) and (b) show the micrographs of sand particles as received and that after the 40th test batch.

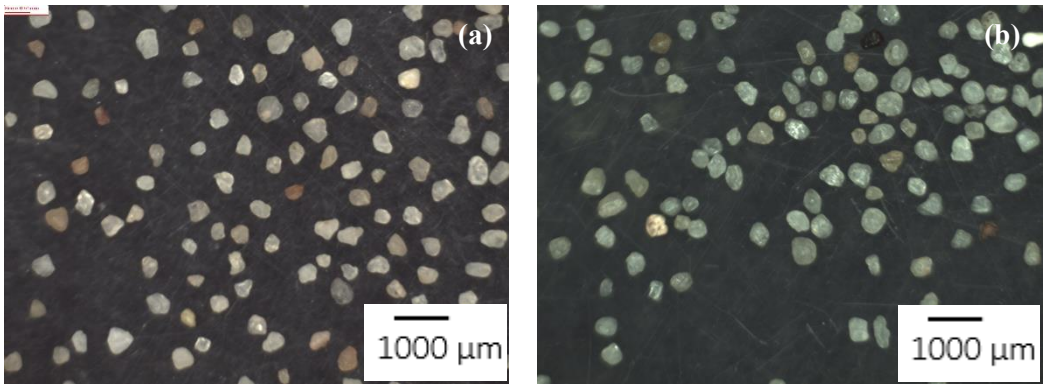

Figure 7 Micrograph of silica sand particles: (a) as received and (b) after the 40th batch of erosion test

The micrographs of sand particles were then analysed using ImageJ. The area of each sand particle was first obtained in ImageJ and the diameter of the sand particle was derived by assuming all sand particles were round. Although this assumption does not apply to all sand particles as seen in Figure 7, it provides the simplicity to approximate particle size distribution as well as to compare particle sizes after repeated test batch under the same assumption.

Figure 8 gives the results for the size distribution of sand particles as received and that after the 40th test batch. Figure 9 shows the results for the average sand diameter after different repeated test batches and the error bar represents 95% confidence limit.

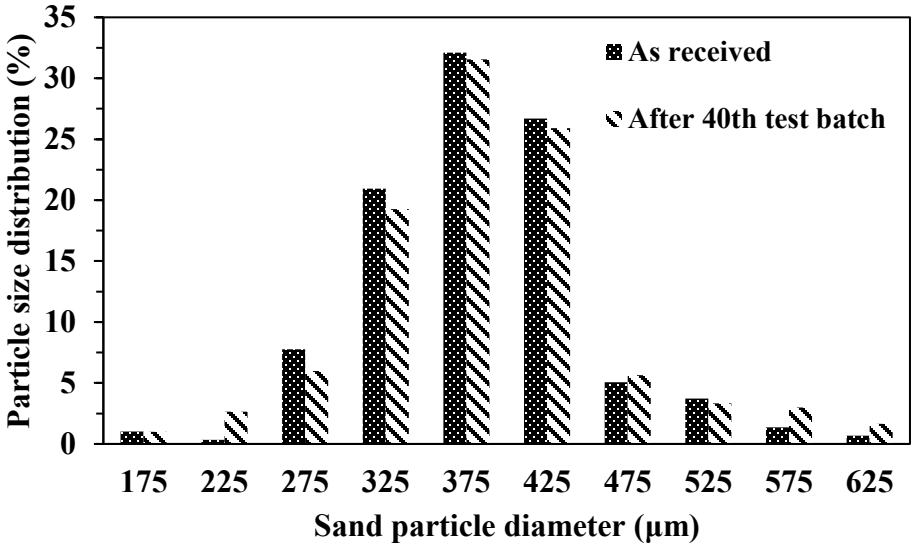

Figure 8 Diameter distribution of sand particle between as received and after the 40th test batch

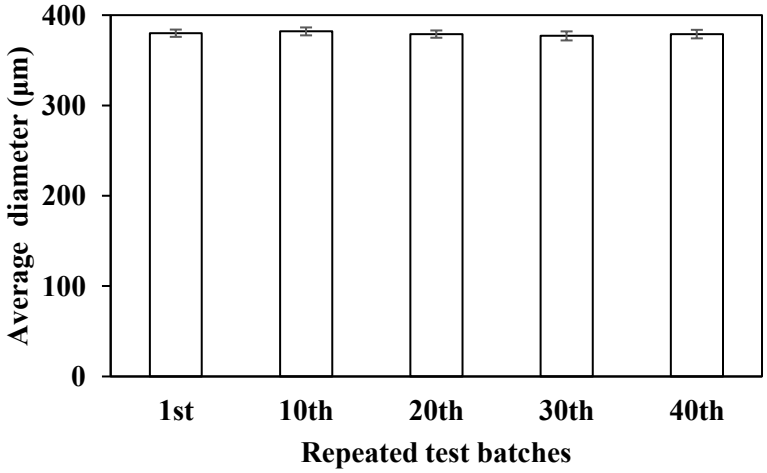

Figure 9 Average diameter of the sand particles after different test batches

As can be seen in Figure 8, there is little difference of size distribution of the sand particles as received and after the 40th test batch. The latter refers to circulating 40 times of a slurry of 400 L of 5wt% sand particles at 30 m/s slurry velocity in the rig. Average diameter of sand particles was represented by the mean of Gaussian distribution analysis based on the particle diameter distribution. As seen in Figure 9, there is

virtually no difference in the average diameter of the sand particles at least up to the 40th test batch as shown in Figure 9. Furthermore, the measured average diameter of received sand particles was found to be 380 μm, which is similar to 392 μm given by the sand supplier.

Angularity of sand particles can play an important role in an erosion process. However, it is difficult to correlate particle angularity with erosion without detailed understanding of both slurry hydrodynamics and impingement behaviour. Since the size of sand particles does not vary significantly as shown in Figure 8 and 9, the effect of angularity change of sand particles on erosion could be utilised to indirectly monitor such change itself if a reference material can be subjected to erosion test with used sand. In this work, a stainless steel 316 was chosen to calibrate the erosive potential of sand particles that had been already pre-used in the 1st, 10th, 20th, 30th, and 40th batch test on a rubber sample.

Figure 10 presents the results with 95% confidence limit for measured material loss in the stainless steel samples using a slurry of used sand particles at an impact angle of 90° and a velocity of 30 m/s.

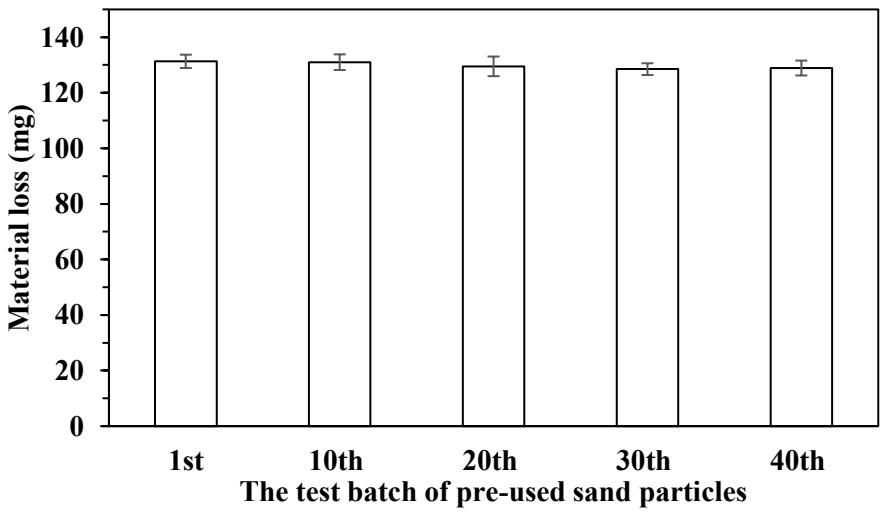

Figure 10 Material loss of stainless steel 316 corresponding to the test batch of pre-used sand particles

It can be clearly seen that there is very little difference in the material loss of the stainless steel 316 after using the slurry with the sand particles pre-used up to 40 times of test batches. Consequently, it can be concluded from the results in Figure 8-10 that the overall erosive potential of the slurry composition and flow conditions used in this work can be maintained by the rig. This leads to the decision that the sand particles can be repeated used in our rig up to at least 40 batches without the need of replacement.

4. Application of slurry-jet erosion test rig

4.1 Slurry-jet erosion testing

Commissioning of the rig was carried out by evaluating the slurry erosion behaviour of a commercial polychloroprene rubber (CR)currently used as lining materials for slurry transport equipment. The rubber contains 50 phr of carbon black and the properties of the CR obtained from the manufacturer are listed in Table 2.

Table 2 Properties of filled polychloroprene rubber used in this study

Properties	
Specific gravity (-)	1.4
Hardness (IRHD)	60
Tensile strength (MPa)	5
Elongation at break (%)	300
Tear strength (N/mm)	20
Compression set (%)	35

Silica sand was supplied by Minerals Marketing (Cheshire, UK) and used as received. The sand is sub-round with an average particle size of the 392 μm, the bulk density of 1.56 g/cm^3 and hardness of 7 on the Mohs scale.

The rubber sample was cut from a roll to produce a square slab of length and width of 40 mm and thickness of 12 mm. The sample thickness was more than 30 times greater than the particle size in order to avoid the substrate effects during a slurry impingement test [30]. Furthermore, the rubber sample must be firmly

secured during testing in order to prevent energy dissipation associated with bulk sample displacement [30]. This was achieved by carefully taping the sample down on a 5mm thick stainless steel substrate using thin adhesive carbon discs . The sample bonded to the metal substrate was then transferred on to a rigid sample holder and subsequently screw-fixed by two metal strips on both sides of the exposed sample surface leaving the sufficient middle area for slurry impingement as shown in Figure 11. Internal diameter of slurry jet nozzle was 4 mm, and distance between the nozzle and the sample surface was kept at 30 mm. The impact angle can be varied by changing the sample holder with a slop of different angle.

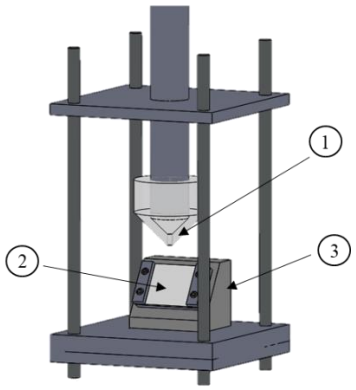

1. Nozzle
2. Sample secured in the sample holder
3. Sample holder

Figure 11 3D schematic of rubber sample fixture for slurry-jet erosion test

Table 3 summaries parameters adopted for testing the polychloroprene rubber in the SJET rig as shown in Figure 1.

Table 3 Parameters of slurry-jet erosion characterisation used in this study

Parameters	
Impact angle (°)	10, 15, 20, 30, 45, 60 and 90
Slurry velocity (m/s)	30
Fluid medium	Fresh tap water
Sand content (wt%)	5
Particle average grain size (μm)	392
Standoff distance (mm)	30
Test temperature (°C)	20±2
Mass of erodent particles (kg)/ Erosion time (h)	Depending on the steady-state of material loss of the specimen

A typical testing procedure involves the following basic steps. 1) Weigh a dry sample via precision scale with an accuracy of ±0.01 mg. 2) Mount the sample in the SJET rig. 3) Conduct the slurry erosion test at pre-determined velocity, impact angle, and the amount of impingement sand. 4) Dismount the tested sample from the rig and condition it according to ASTM G73. 5) Weigh the tested and conditioned sample.

Figure 12 present the results for weight change as a function of conditioning time after the erosion test and the error bar is 95% confidence limit.

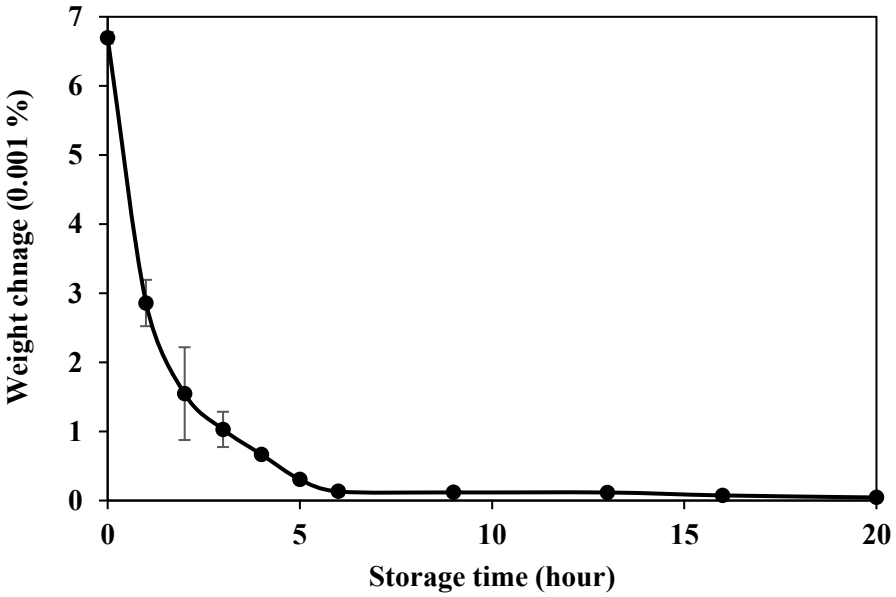

Figure 12 Weight change of rubber specimen as a function of conditioning time

It can be seen that the rubber experiences extremely small amount of weight loss during 20 hours of conditioning due to water evaporation. As a result, All rubber samples after the SJET erosion tests had been conditioned for 16 hours before they were weighed.

4.2 Cumulative material loss

Figure 13 shows the results for cumulative material loss in the polychloroprene rubber (CR) as a function of the mass of impingement sand after the tests following the procedure described in 4.1.

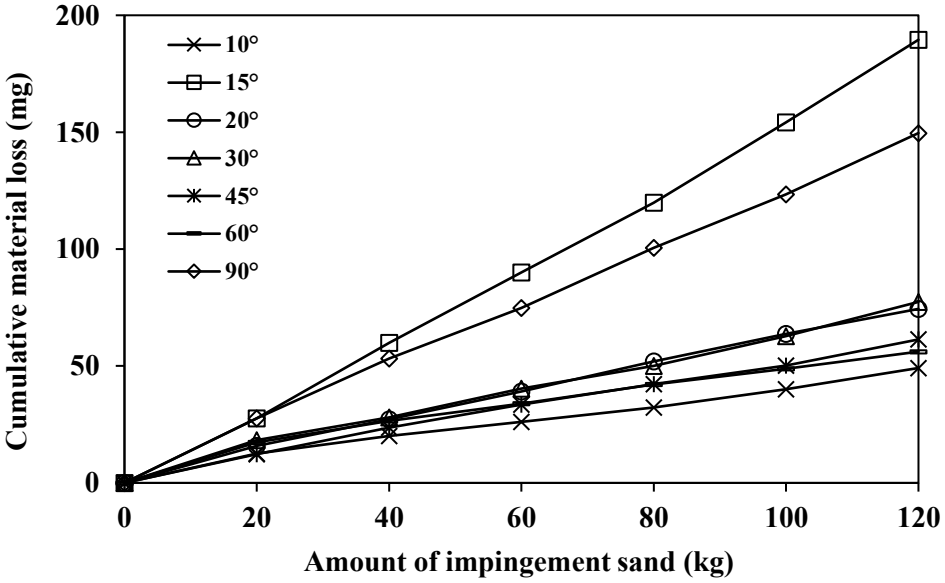

Figure 13 Cumulative mass loss of polychloroprene rubber as a function of the amount of impingement sand in slurry erosion tests at impact angles from 10° to 90°

As can be seen, mass loss due to slurry erosion is linearly proportional to the mount of impingement sand at all impact angles. Furthermore, the results in Figure 13 indicate that the most material loss tend to be found at an impact angle of 15°. It is also interesting to see that the material loss at 90° impact angle is less than that at 15° impact angle but is higher than all other intermediate impact angles. This suggests that material removal of the CR is probably controlled by different erosion mechanisms between glancing and normal impact angle

In order to demonstrate the reproducibility of the developed SJET rig and testing protocol, the erosion test was repeated with the same CR at impact angles of 15°, 30°, 45° and 90°. All other test conditions were

kept the same as in Table 3. The results for the cumulative material loss obtained from both tests are compared in Figure 14.

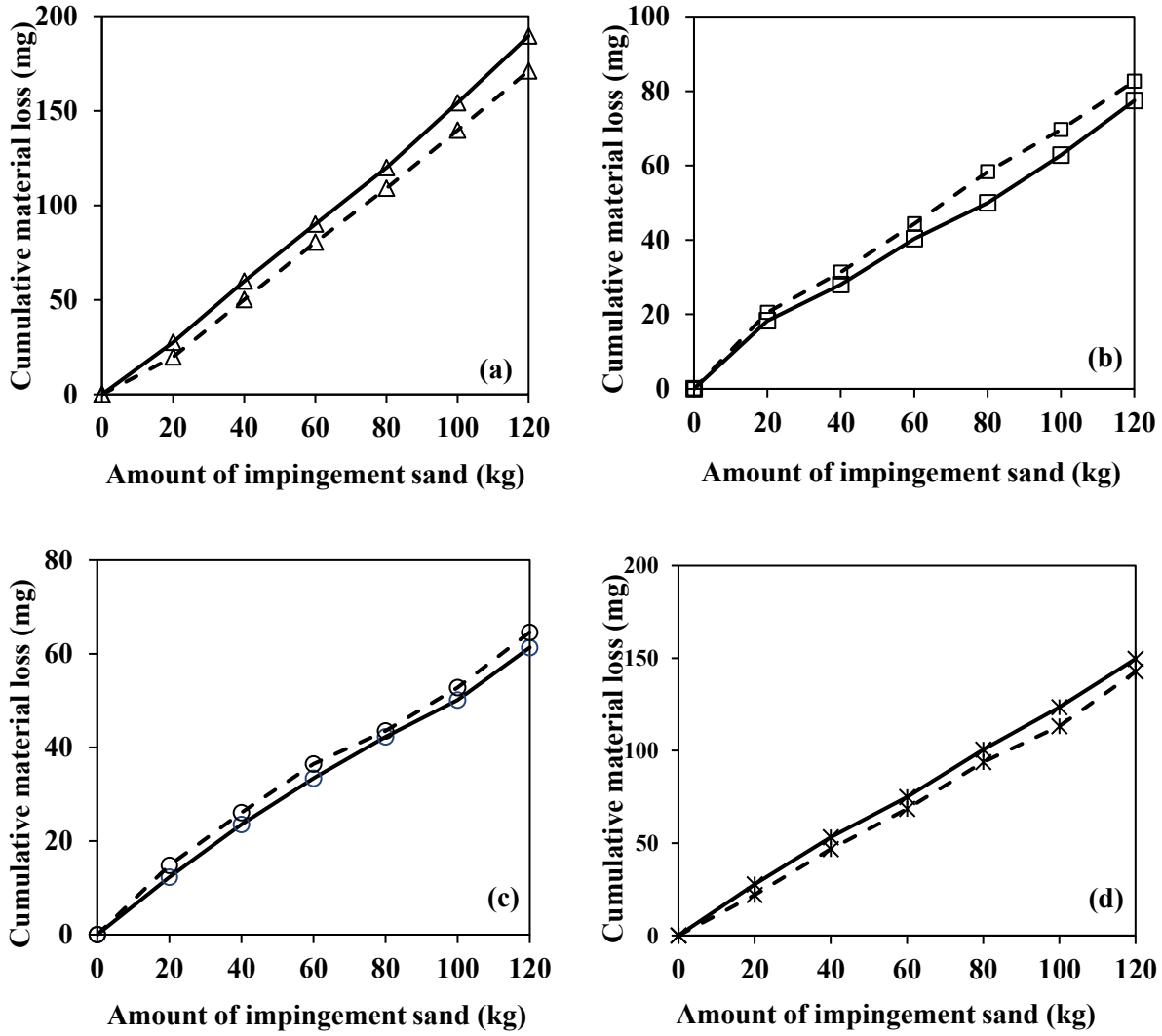

Figure 14 Cumulative mass loss of polychloroprene rubber as a function of the amount of impingement sand in slurry erosion tests at impact angles of (a) 15°, (b) 30°, (c) 45° and (d) 90°; solid line represents the first test and dash line for the repeat

It can be seen that the material losses of CR measured in two individual tests are closed to each other and a variation of less than 10% is observed across all four different angles and the amount of impingement sand. It should be noted that the variation in mass loss could also be partly attributed to inconsistent rubber surface features resulting from bulk production.

4.3 Effect of impact angles on erosion rate

In this study, the erosion rate was defined as the mass of rubber removed by per unit mass of erodent sand. Thus, the erosion rate of rubber specimens can be obtained directly from the slope of the linear portion of the graphs in Figure 13 and 14. As a result, Figure 15 shows the erosion rate as a function of impact angle for the rubber.

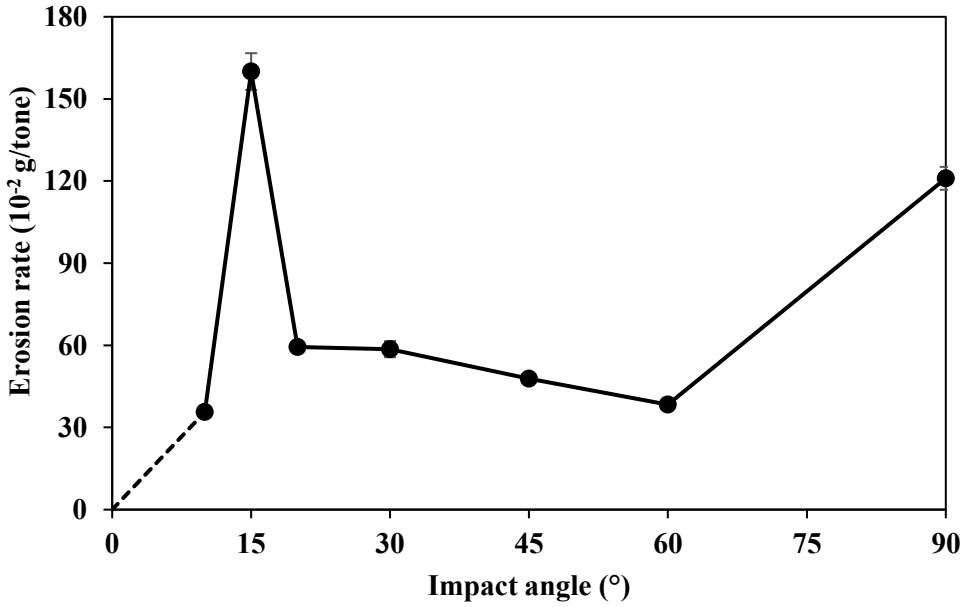

Figure 15 Rate of erosion as a function of impact angle for polychloroprene rubber

The correlation in Figure 15 exhibited relatively higher erosion wear at glancing impact angle, which is commonly noticed for a ductile material eroded by angular particles. The highest erosion rate for the CR used in this work was found at 15° and the rate experiences a sharp increase and decrease with 5° apart from 15° impact angle. It implies the test rig and procedure possess an adequate resolution to capture abrupt changes in the erosion rate of elastomeric materials. For the CR, the influence of impact angles is much less significant between 20° and 60°. However, another peak of erosion rate can be observed when the

impact angle is approaching normal impact at 90°. These results are consistent with those obtained by the literature [1,10] and will be further discussed in the next section. The dual-peak phenomenon observed in Figure 15 suggests that there could be at least two different erosion mechanisms operating at glancing and normal impact angles. The parallel and normal velocity components of impingement sand were likely responsible for these differences with the former causing the lateral displacement of the material and the latter resulting in a vertical indentation. It can be seen in Figure 16 that surface damage of the CR after 10° and 90° erosion tests transformed from an elliptical ploughing pattern at the lower impact angle to a more rounded crater at a normal incidence. Such transition highlights the dominance of parallel and normal impact vector at these two different impact angles.

Figure 16 shows wear scars of eroded surface using both optical and SEM imaging.

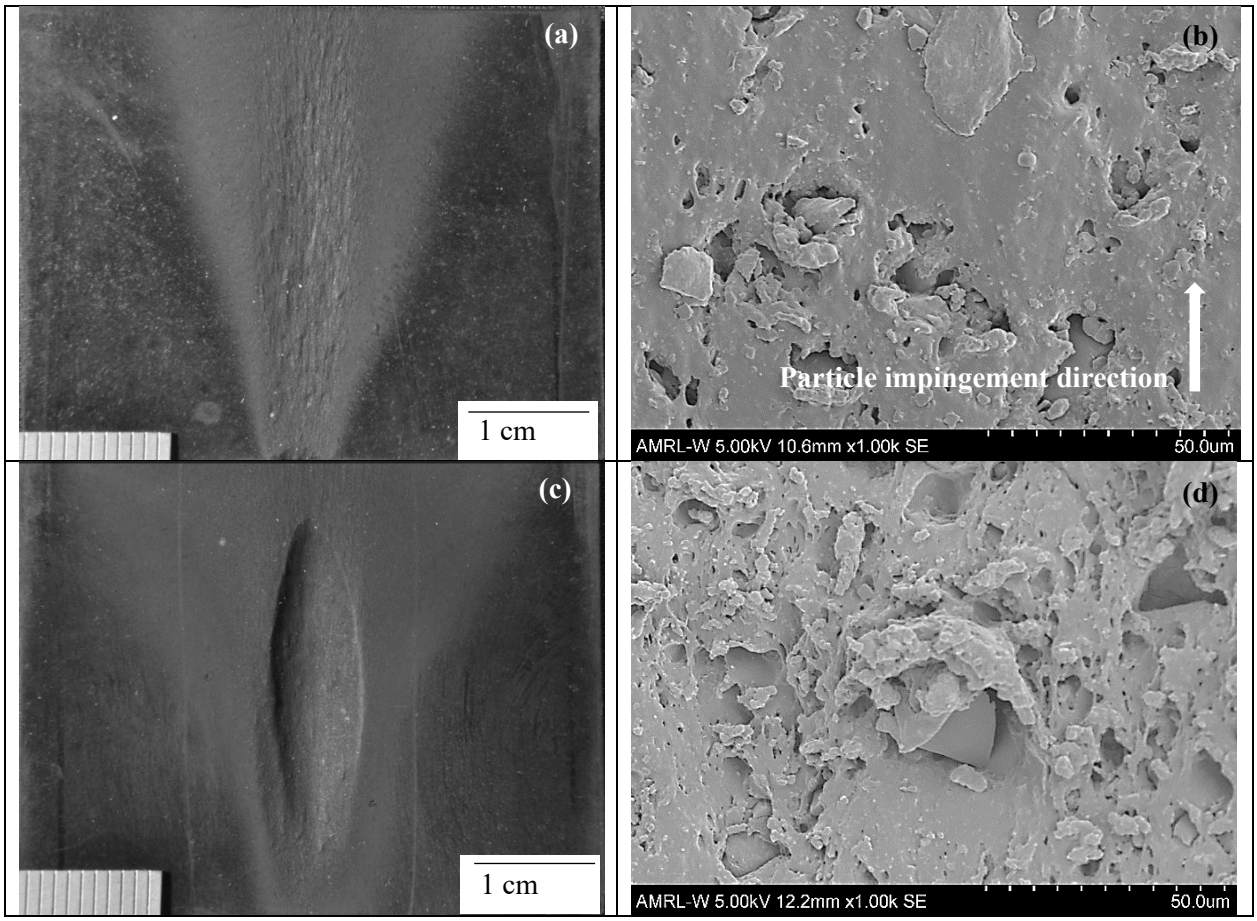

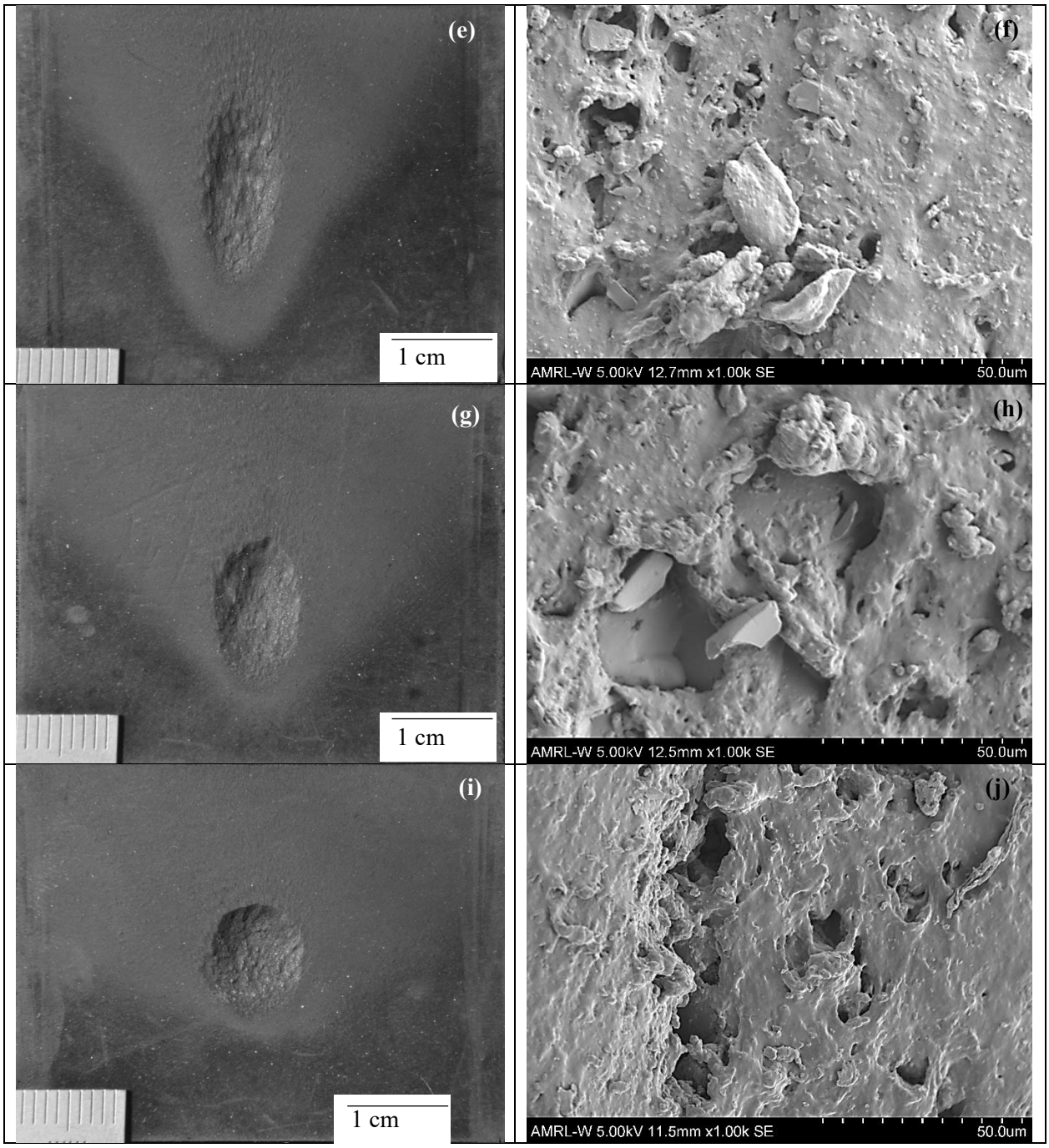
(e)
1 cm
(f)
AMRL-W 5.00kV 12.7mm x1.00k SE
50.0um
(g)
1 cm
(h)
AMRL-W 5.00kV 12.5mm x1.00k SE
50.0um
(i)
1 cm
(j)
AMRL-W 5.00kV 11.5mm x1.00k SE
50.0um

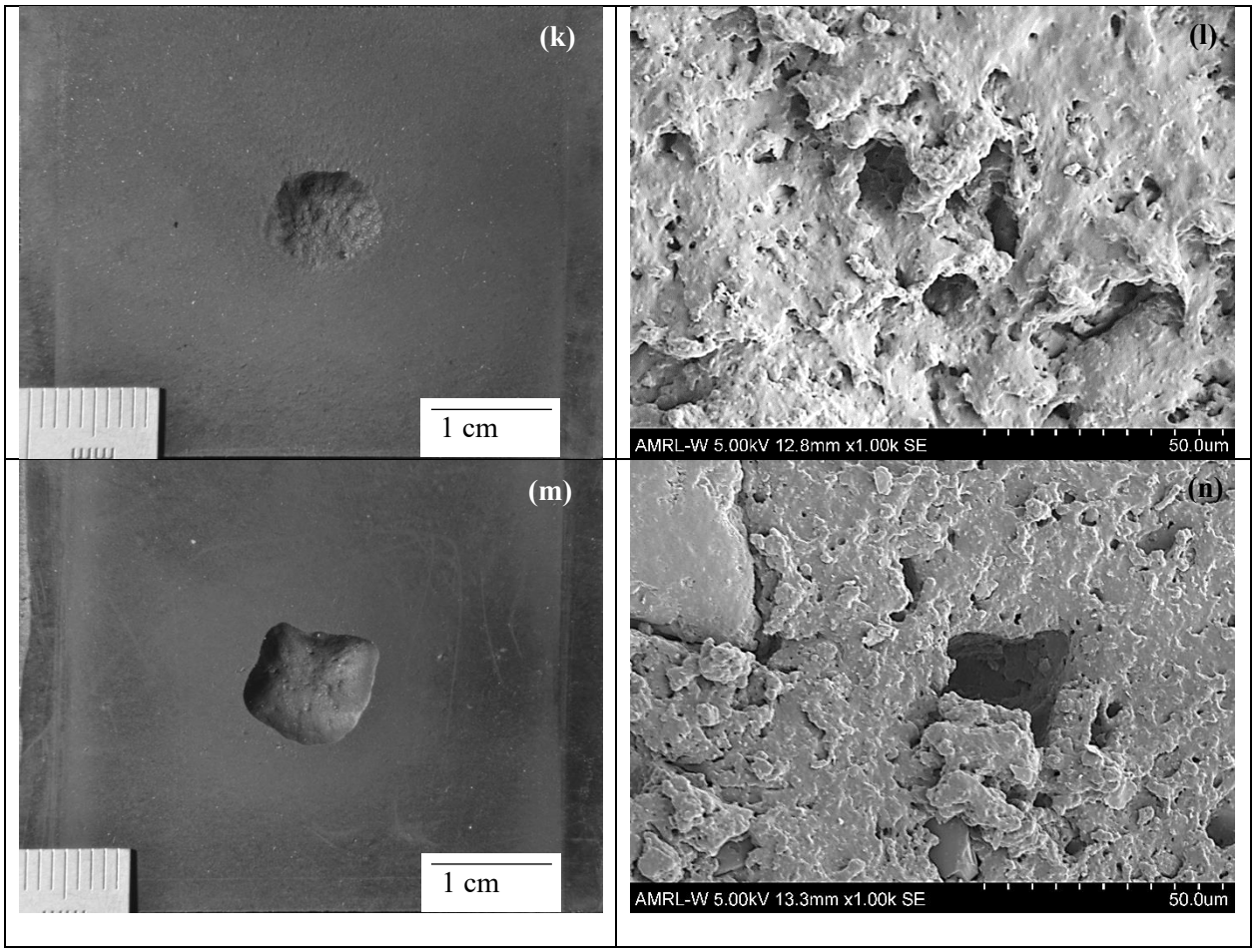

Figure 16 Optical and SEM micrographs of eroded surface of polychloroprene rubber at impact angle of 10° (a-b), 15° (c-d), 20° (e-f), 30° (g-h), 45° (i-j), 60° (k-l), and 90°(m-n)

It can be seen from the optical images that eroded area transforms from an elongated shape toward a circle shape as the impact angle increases. This is expected from the change of the impingement area corresponding to different impact angles. Although it is not possible to quantify the depth of the wear scars through 2D imaging, Figure 16 seems to suggest that the wear scars evolve from a large shallow area to a small deep area as the slurry impact changes from a glancing to a normal angle. At lower impact angles, the parallel component of sand velocity was higher than the normal component and there is a higher probability for the erodent sand to roll and slide on the rubber surface. Consequently, sand particles were unable to penetrate deeply into the rubber surface and the material is removed mainly through a ploughing, or shearing, mechanism as shown in Figure 16 (b, d, f and h). In contrast, at normal impact angle, the normal

component of the kinetic energy of impingement particles is absorbed by the rubber surface. When it is associated with the repeated impact, the deformation wear will occur. As the Poisson's ratio of rubber is around 0.5, surface tensile stress can be generated when the rubber is impacted locally at a normal angle. The surface tensile stress can initiate the progressive development of fine cracks into the eroded rubber surface, and when these cracks intersect, the material loss can occur. In Figure 16 (n), the indentation craters were detected where the material was displaced by deformation around the crater and formed a rim. The rim was flattened and fractured upon further impact. As a result, deformation wear tends to be prevailing at normal impact angle and leads to a high erosion rate as seen in Figure 15. For impact angles below 15°, the probability for the impingement sand particles slip and roll over rubber surface increases and this could be particularly the case in wet erosion wear. This could account for a very low erosion rate at 10° impact angle. At impact angles between 20° and 60°, the sand particles may stop sliding and rolling before they lose contact with rubber surface. This can be considered as the point at which tangential velocity of impingement particles becomes close to zero and the sand particles are more likely to bounce off the rubber surface after the impact. This means less energy absorbed by the rubber at these impact angles and reduced erosion rate could be observed as in Figure 15.

It is also worth noting that the wear scar generated at the impact angle of 90° in Figure 16 (m) is not particularly circular. A model proposed by Benchaita et al. [31] suggests that for a normal incidence of a slurry jet, the particles impact the surface at 90° in the centre of the impingement area but their impact angles start to deviate from 90° with increasing distance from the centre. In addition, when the wear scar becomes deep enough such as that at 90°, sand particles rebounded from the centre could impinge the surrounding region of eroded scars at a somewhat arbitrary angles. These may explain why the wear scar does not appear to be particular circular at 90° impact angle.

4.4 Comparison with erosion modelling

The literature has shown that the maximum erosion wear caused by liquid-solid slurry for ductile materials are typically found at impact angles between 15° and 50°, whereas brittle materials such as glass tend to have a maximum material loss due to slurry erosion at normal impact at 90° [13,18,21,25,32–35]. Bitter proposed two different theoretical models to estimate the erosion caused by gas-solid flow [36,37]. One was used to determine the material loss due to cutting mechanism and the other due to deformation wear. This method was adopted by Neilson and Gilchrist and they considered that the total mass loss at a normal impact angle was due to the deformation wear only and proportional to the kinetic energy correlated with the normal component of impact velocity, above a threshold [38]. The deformation wear can be, therefore, calculated using Equation (6)

$$W_D = \frac{M\,(V \sin\alpha - K)^2}{2\varepsilon} \qquad (6)$$

where W_D (kg) is deformation wear produced by M kilogram of particles at an impact angle α and particle velocity V (m/s). K (m/s) is the normal component of particle impact velocity, below which there is no erosion occurs. In general, K is neglected, as it is very small compared to the impact velocity. ε is specific energy (J mg^{-1}), required to remove one-unit mass of material by deformation wear and is assumed to be constant for a specific material.

According to Neilson and Gilchrist, the mass loss due to cutting wear can be obtained by subtracting deformation wear from the total wear measured [38]. The cutting wear was analysed similarly based on an approximation of kinetic energy, determined from the tangential particle velocity. Adjustable parameters were also used to narrow the experimental variation of cutting wear with impact angles. Thus, expressions for the cutting wear, W_c (kg) as a function of impact angle are

$$W_C = \frac{M\,V^2 \cos^2\alpha \sin n\alpha}{2\Phi} \qquad \text{for } \alpha < \alpha_0 \qquad (7)$$

$$W_C = \frac{M\,V^2 \cos^2\alpha}{2\Phi} \qquad \text{for } \alpha > \alpha_0 \qquad (8)$$

$$\text{when } \alpha = \alpha_0, \sin n\alpha_0 = 1, \text{ i.e. } \alpha_0 = \frac{\pi}{2n} \qquad (9)$$

where Equations 7 and 8 are cutting wear at small and large impact angles. α_0 is the impact angle at which the residual parallel component of particle velocity becomes zero rendering Equation 7 and 8 to predict the same material loss. *n* in Equation 9 is a constant depending on the material properties and testing conditions. Φ is specific energies (J mg^{-1}) for cutting wear.

In order to further understand the effect of slurry impact angles on the CR erosion rate obtained in this study, the components of deformation and cutting wear were calculated using Equations 6-9 following the procedure proposed by Neilson and Gilchrist [38]. This gives the correlation between erosion rate and impact angle as shown in Figure 17.

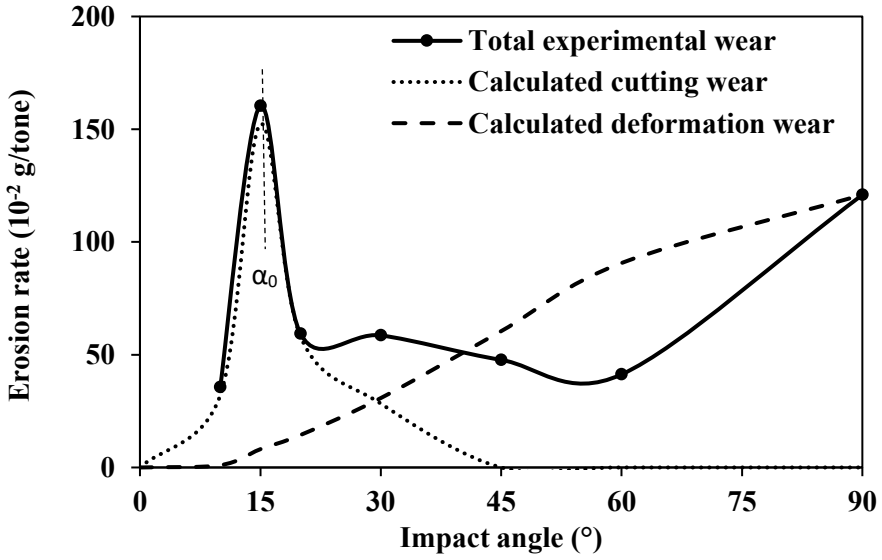

Figure 17 Comparison of erosion rate as a function of impact angle for polychloroprene rubber between experimental measurement and calculated value

The results for erosion parameters for the filled polychloroprene rubber characterised under our test conditions include *Φ=36 (J/mg)*, *ε=361 (J/mg), α_0=16.1 (°)*, and *n=5.58*. The calculated results for cutting and deformation wear in Figure 17 reveal that there are two peaks of erosion rate caused by distinct wear

mechanisms. One is found at an impact angle of 16.1° caused by cutting wear and this agrees well with the highest erosion rate at 15° observed in our experiment results. The other peak can be found at normal impact angle based on the calculated deformation wear and this also agrees with the experimental results in this work. In addition, the erosion wear model expressed by Equation 6-9 can also seem to depict the evolution of two different wear mechanisms a function impact angles as shown in Figure 17. The erosion rate obtained from superimposition of these two wear mechanisms tends to have an excellent agreement with the experimental results except in the range of impact angles after 45 and before 90°. This discrepancy is mainly due to the fact that the model fails to take into account particle rebound, which is much more prevailing at the intermediate impact angles than at either glancing or normal impact angles. Further work is required to consider this effect for improved modelling of rubber erosion behaviour.

Nevertheless, the model helps to illustrate the key erosion mechanisms controlling rubber erosion characteristics. For instance, α_0 =16.1° implies that the particles left the CR surface without any residual parallel component of particle velocity when the sand particles impacted the CR at impact angles higher than 16.1°. The significantly lower value of Φ, compared to ε, emphasises that cutting wear is the dominant process in CR at small impact angles as generally found for ductile materials. The gained values of specific energies to remove the material in erosion for both cutting and deformation wear can be useful parameters for predicting and comparing the erosion resistance of elastomeric materials.

5. Conclusion

The development of a slurry-jet erosion test rig has been described and proves to be a useful alternative to existing methods for laboratory-scale investigation of slurry erosion beaviour of elastomeric materials. The new SJET rig has advantages of simple construction and easy operation without compromising on the accurate control of a wide range of testing parameters. In addition, using large slurry reservoirs facilitates the slurry erosion testing in a sizable batch scale and prevents the increase of slurry temperature over a large number of test batches. The impact velocity and slurry composition were found to be consistent with the

set values and characteristics of sand particles had a negligible change after passing through a pump. Consequently, the slurry erosion of elastomers in different service conditions can be characterised accurately and reproducible by varying suitable test parameters.

Test results for a case study using a filled polychloroprene rubber have shown the SJET rig is capable of distinguishing key mechanisms during rubber erosion. The results for erosion rate at different impact angles were consistent with those found in the literature. Polychloroprene rubber showed an abrupt change in erosion rate at oblique impact angles and reached a peak value at a glancing impact angle of 15°. This is followed by a much less dependence of impact angles at the intermediate range until the impact angle is approaching 90°. In addition, the experimental results for erosion rate at both low and high impact angles correlate well with a theoretical model based on dissipation of impact kinetic energy. The model produced several erosion parameters that are useful for comparing and predicting the erosion behaviour and resistance of rubber materials.

Acknowledgement

The authors would like to express their great gratitude to the Royal Thai Government and The Weir Group PLC for financial support to this work. We would also like to thank reviewers for their valuable comments.

Reference

[1] J.C. Arnold, I.M. Hutchings, The Erosive Wear of Elastomers, J. Rubber Res. 6 (1991) 241–256.

[2] L.C. Jones, Low angle scouring erosion behaviour of elastomeric materials, Wear. 271 (2011) 1411–1417. https://doi.org/10.1016/j.wear.2010.12.057.

[3] Y. Xie, J. (Jimmy) Jiang, K.Y. Tufa, S. Yick, Wear resistance of materials used for slurry transport, Wear. 332–333 (2015) 1104–1110. https://doi.org/10.1016/j.wear.2015.01.005.

[4] J.C. Arnold, I.M. Hutchings, The Mechanisms of Erosion of Unfilled Elastomers by Solid Particle Impact, Wear. 138 (1990) 33–46.

[5] I.R. Sare, J.I. Mardel, A.J. Hill, Wear-resistant metallic and elastomeric materials in the mining and mineral processing industries—An overview, Wear. 250 (2001) 1–10. https://doi.org/10.1016/S0043-1648(01)00622-6.

[6] Y. Xie, J. (Jimmy) Jiang, M.A. Islam, Elastomers and plastics for resisting erosion attack of abrasive/erosive slurries, Wear. 426–427 (2019) 612–619. https://doi.org/10.1016/j.wear.2019.01.123.

[7] A.H. Hutchings, I. M., Deuchar, D.W.T., Muhr, Erosion of Unfilled Elastomers by Solid Particle Impact, J. Mater. Sci. 22 (1987) 4071–4076. https://doi.org/10.1016/0043-1648(90)90166-8.

[8] J.C. Arnold, I.M. Hutchings, Flux rate effects in the erosive wear of elastomers, J. Mater. Sci. 24 (1989) 833–839. https://doi.org/10.1007/BF01148765.

[9] J. Li, I.M. Hutchings, Resistance of cast polyurethane elastomers to solid particle erosion, Wear. 135 (1990) 293–303. https://doi.org/10.1016/0043-1648(90)90032-6.

[10] J.C. Arnold, I.M. Hutchings, A model for the erosive wear of rubber at oblique impact angles, J. Phys. D. Appl. Phys. 25 (1992) A222–A229. https://doi.org/10.1088/0022-3727/25/1A/034.

[11] W. Tsai, J.A.C. Humphrey, I. Cornet, A. V. Levy, Experimental measurement of accelerated erosion in a slurry pot tester, Wear. 68 (1981) 289–303. https://doi.org/10.1016/0043-1648(81)90178-2.

[12] R. Gupta, S.N. Singh, V. Seshadri, Prediction of uneven wear rate in a slurry pipeline on the basis of measurements in a pot tester, Bulk Solids Handl. 15 (1995) 169–178.

[13] J.B. Zu, I.M. Hutchings, G.T. Burstein, Design of a slurry erosion test rig, Wear. 140 (1990) 331–344. https://doi.org/10.1016/0043-1648(90)90093-P.

[14] J.J. Tuzson, Laboratory Slurry Erosion Tests and Pump Wear Rate Calculations, J. Fluids Eng. 106 (2009) 135. https://doi.org/10.1115/1.3243089.

[15] H.M.I. Clark, J. Tuzson, K.K. Wong, Measurements of specific energies for erosive wear using a Coriolis erosion tester, Wear. 241 (2000) 1–9. https://doi.org/10.1016/S0043-1648(00)00327-6.

[16] H.M. Hawthorne, Y. Xie, S.K. Yick, A new Coriolis slurry erosion tester design for improved

slurry dynamics, Wear. 255 (2003) 170–180. https://doi.org/10.1016/S0043-1648(03)00060-7.

[17] F.Y. Lin, H.S. Shao, Effect of impact velocity on slurry erosion and a new design of a slurry erosion tester, Wear. 143 (1991) 231–240. https://doi.org/10.1016/0043-1648(91)90098-F.

[18] Y. Iwai, K. Nambu, Slurry wear properties of pump lining materials, Wear. 210 (1997) 211–219. https://doi.org/10.1016/S0043-1648(97)00055-0.

[19] S. Turenne, M. Fiset, J. Masounave, The effect of sand concentration on the erosion of materials by a slurry jet, Wear. 133 (1989) 95–106. https://doi.org/10.1016/0043-1648(89)90116-6.

[20] Y. Naerheim, Material Removal Mechanism of Ni(200) When Eroded by A Slurry at 30 Incidence, Wear. 105 (1985) 123–130.

[21] J.B. Zu, G.T. Burstein, I.M. Hutchings, A comparative study of the slurry erosion and free-fall particle erosion of aluminium, Wear. 149 (1991) 73–84. https://doi.org/10.1016/0043-1648(91)90365-2.

[22] Y. Li, G.T. Burstein, I.M. Hutchings, The influence of corrosion on the erosion of aluminium by aqueous silica slurries, Wear. 186–187 (1995) 515–522. https://doi.org/10.1016/0043-1648(95)07181-4.

[23] R.J.K. Wood, B.G. Mellor, M.L. Binfield, Sand erosion performance of detonation gun applied tungsten carbide/cobalt-chromium coatings, Wear. 211 (1997) 70–83. https://doi.org/10.1016/S0043-1648(97)00071-9.

[24] Q. Fang, H. Xu, P.S. Sidky, M.G. Hocking, Erosion of ceramic materials by a sand/water slurry jet, Wear. 224 (1999) 183–193. https://doi.org/10.1016/S0043-1648(98)00309-3.

[25] G.T. Burstein, K. Sasaki, Effect of impact angle on the slurry erosion-corrosion of 304L stainless steel, Wear. 240 (2000) 80–94. https://doi.org/10.1016/S0043-1648(00)00344-6.

[26] J. Suchánek, V. Kuklík, E. Zdravecká, Influence of microstructure on erosion resistance of steels, Wear. 267 (2009) 2092–2099. https://doi.org/10.1016/j.wear.2009.08.004.

[27] H.S. Grewal, A. Agrawal, H. Singh, Design and development of high-velocity slurry erosion test rig using CFD, J. Mater. Eng. Perform. 22 (2013) 152–161. https://doi.org/10.1007/s11665-012-

0219-y.

[28] H.S. Grewal, H.S. Arora, A. Agrawal, H. Singh, S. Mukherjee, Slurry erosion of thermal spray coatings: Effect of sand concentration, Procedia Eng. 68 (2013) 484–490. https://doi.org/10.1016/j.proeng.2013.12.210.

[29] H.S. Grewal, A. Agrawal, H. Singh, B.A. Shollock, Slurry Erosion Performance of Ni-Al 2 O 3 Based Thermal-Sprayed Coatings : Effect of Angle of Impingement, J. Therm. Spray Technol. 23 (2014) 389–401. https://doi.org/10.1007/s11666-013-0013-x.

[30] E. Southern, A.G. Thomas, The Impact of Rigid Spheres on Rubber, J. Appl. Polym. Sci. 16 (1972) 1641–1651.

[31] M.T. Benchaita, P. Griffith, E. Rabinowicz, Erosion of metallic plate by solid particles entrained in a liquid jet, J. Manuf. Sci. Eng. Trans. ASME. 105 (1983) 215–222. https://doi.org/10.1115/1.3185891.

[32] Y. Li, G.T. Burstein, I.M. Hutchings, Influence of environmental composition and electrochemical potential on the slurry erosion-corrosion of aluminium, Wear. 181–183 (1995) 70–79. https://doi.org/10.1016/0043-1648(95)90010-1.

[33] G.R. Desale, B.K. Gandhi, S.C. Jain, Effect of erodent properties on erosion wear of ductile type materials, Wear. 261 (2006) 914–921. https://doi.org/10.1016/j.wear.2006.01.035.

[34] H.M.I. Clark, K.K. Wong, Impact angle, particle energy and mass loss in erosion by dilute slurries, Wear. 186–187 (1995) 454–464. https://doi.org/10.1016/0043-1648(95)07120-2.

[35] V. Javaheri, D. Porter, V.T. Kuokkala, Slurry erosion of steel – Review of tests, mechanisms and materials, Wear. 408–409 (2018) 248–273. https://doi.org/10.1016/j.wear.2018.05.010.

[36] J.G.A. Bitter, A study of erosion phenomena part I, Wear. 6 (1963) 5–21. https://doi.org/10.1016/0043-1648(63)90003-6.

[37] J.G.A. Bitter, A Study of Erosion phenomena: Part II, Wear. 6 (1963) 169–190. https://doi.org/10.1016/0043-1648(63)90073-5.

[38] J.H. Neilson, A. Gilchrist, Erosion by a stream of solid particles, Wear. 11 (1968) 111–122.

https://doi.org/10.1016/0043-1648(68)90591-7.